*Environ. Water Eng., 2025, 11(2), 125-133* DOI: 10.22034/ewe.2024.473908.1961

EWE

**Environment and Water Engineering**

**Homepage: www.jewe.ir**

ISSN: 2476-3683

# Evaluating four interpolation methods of temperature and vegetation indices obtained from satellite images in daily reference evapotranspiration modeling

Parastoo Amirzehni[1], Saeed Samadianfard[1]✉, Amirhossein Nazemi[1], and Ali Ashraf Sadraddini[1]

[1]Department of Water Engineering, Faculty of Agriculture, University of Tabriz, Tabriz, Iran

**ARTICLE INFO**

**Paper Type:** Research Paper

**Received**: 17 August 2024
**Revised:** 23 September 2024
**Accepted**: 24 September 2024
**Published**: 22 May 2025

**Keywords**
Composite Bezier
Cubic Spline
Reference Evapotranspiration
Satellite Images

***Corresponding author:**
S. Samedianfard
✉ s.samadian@tabrizu.ac.ir

**ABSTRACT**

Due to the requirement for extensive meteorological data, the standard FAO Penman-Monteith method for estimating reference evapotranspiration ($ET_0$) is limited. Moreover, the lack of sufficient meteorological data in many regions has led to the utilization of remote sensing imagery as a valuable alternative. However, these images often have multi-day temporal resolutions. To obtain daily remote sensing data, in this study four mathematical functions: spline (S), cubic spline (CS), Bezier (B), and composite Bezier (CB) for interpolating 8-day land surface temperature (LST-D/N) and 16-day vegetation indices (NDVI and LAI) to daily values were compared. Subsequently, four remote sensing variables were used as inputs under 12 scenarios for two neural network models: Multi-Layer Perceptron (MLP) and Multi-Layer Perceptron combined with Stochastic Gradient Descent (MLP-SGD) to estimate $ET_0$. This study was conducted at two stations, Urmia and Kerman, from 2001 to 2022. The determination coefficients of 0.89 in Urmia and 0.83 in Kerman demonstrated the superiority of spline-based interpolation methods in estimating $ET_0$. Spline functions are recommended for interpolating remote sensing variables to estimate reference evapotranspiration.

**How to cite this paper:**
Amirzehni, P., Samadianfard, S., Nazemi, A., & Sadradini, A. (2025). Evaluating four interpolation methods of temperature and vegetation indices obtained from satellite images in daily reference evapotranspiration modeling. *Environ. Water Eng.*, *11*(2), 125-133. doi: 10.22034/ewe.2024.473908.1961

## 1. Introduction

Evapotranspiration (ET) is the second main component of the hydrological cycle, as it returns more than 60% of global precipitation to the atmosphere (Falamarzi et al., 2014). In the hydrological cycle and the agricultural process, reference evapotranspiration ($ET_0$) is one of the most important factors, and its accurate estimation is crucial for the design, planning, and optimal management of irrigation systems and other efficient water resource management (Ferreira et al., 2019). Although several statistical methods have been studied worldwide to estimate this parameter, the FAO Penman-Monteith (FAO56-PM) equation is considered the only reference mathematical method for calculating $ET_0$ by the Food and Agriculture Organization (FAO) of the United Nations (Pereira et al., 2015). Ebrahimipak et al. (2018) used meteorological data to calibrate grass lysimetry data in the Qazvin region and concluded that the FAO Penman-Monteith is the best estimation method with higher accuracy in estimating reference evapotranspiration. Ahmadpari et al. (2019) also conducted a study in Khorramabad County to compare evapotranspiration methods and determine the most suitable method for estimating reference evapotranspiration. Their results showed that the FAO Penman-Monteith method had the highest accuracy.

The FAO Penman-Monteith method requires a wide range of climatic data to calculate ET. The inherent complexity of this method in determining ET makes its practical use for precise irrigation water management difficult (Aghelpour et al., 2022b). The main reason for the lack of use of ET in general and smart irrigation is the complexity and unavailability of climatic information in the agricultural area (Popovic et al. 2023). Simplifying ET estimation with a limited number of meteorological data is the core of productivity and sustainability in agriculture (Keshtegar et al., 2022). In recent years, the use of machine learning (ML) models for estimating and predicting evapotranspiration has been employed. These models, also known as black-box models, can discover

complex numerical relationships between input and target variables with high accuracy.

Hashemi and Sepaskhah (2019) used an artificial neural network model and considered the results of the FAO Penman-Monteith equation as a basis, to estimate the daily evapotranspiration of barley crops at an agricultural research station at Shiraz University, Iran. The results were confirmed by weighing lysimeters, and due to the accuracy and compatibility with the limitations of climatic data, the superior performance of the studied model was reported. Their results showed that in the multilayer perceptron model, the crop evapotranspiration is more sensitive to sunshine hours and less sensitive to wind speed. Accurate calculation of evapotranspiration leads to reduced water losses and better water planning.

Land surface temperature (LST) derived from satellite imagery is crucial for retrieving terrestrial evapotranspiration (ET). Based on this, Amirzehni et al. (2023). considering the capability of artificial neural networks in the computational analysis of complex processes, conducted a study aiming to apply this technology for analyzing effective data in estimating $ET_0$ using 20-year daily meteorological data from Tabriz weather station. For modeling $ET_0$, the input set to the artificial neural networks included values of minimum and maximum temperature, minimum and maximum relative humidity, wind speed, saturated vapor pressure, and sunshine hours, as well as remote sensing variables including day and night land surface temperature, LAI (Leaf Area Index), and NDVI. The results showed that the artificial neural network with an $R_2$ of about 0.98 is a very suitable method for $ET_0$ analysis. At Tabriz station, the variables of saturated vapor pressure and night LST (Land Surface Temperature) were reported as the most effective, and wind speed and NDVI as the least effective variables in estimating $ET_0$. Bellido et al. (2023) studied data from 122 automatic weather stations in different regions in southern Spain from 1999 to 2022 and evaluated four machine learning models: Multi-Layer Perceptron (MLP), Extreme Learning Machine (ELM), Random Forest, and Support Vector Machines. The results showed that MLP consistently outperformed the conventional Hargreaves-Samani method in estimating $ET_0$ in all cases. Walls et al. (2020) compared the Stochastic Gradient Descent (SGD) model with seven Artificial Neural Network (ANN) models for predicting daily evapotranspiration in Oxford, Canada, from April to July 2018. They used net radiation, air temperature, soil heat flux, and wind speed as input variables and concluded that the SGD learning algorithm had better performance (Aghelpour et al., 2022a). Dimitriadis and Nikolakopoulos (2022) used data from 62 meteorological stations in Greece during 2016-2019 to estimate $ET_0$. The inputs were mean temperature ($T_{mean}$), sunshine hours (N), solar radiation ($R_s$), net radiation ($R_n$), vapor pressure deficit ($e_s$-$e_a$), wind speed ($u_2$), and elevation (Z). They ran nineteen Multi-Layer Perceptron (MLP) models and compared the results with Penman-Monteith FAO estimates. They concluded that the MLP model with all variables as inputs had better performance than the other models.

One of the complications of using satellite images in discrete management and planning is the discontinuity and multi-day intervals of these images, which in practice makes continuous monitoring impossible. On the other hand, no precise research has been done on comparing the types of interpolation methods on satellite images with the application of combining multi-layer perceptron with stochastic gradient descent. This research aimed to investigate the performance of four interpolation functions, spline, cubic spline, Bezier, and composite Bezier, in the temporal interpolation of satellite images and modeling reference evapotranspiration using MLP and MLP-SGD methods.

## 2. Materials and Methods

### 2.1 Study area

In this research, meteorological and remote sensing data from two stations in Urmia and Kerman were used (Fig. 1). The city of Urmia is located in northwestern Iran, which is classified as a semi-arid and cold-arid region in terms of climate and is also classified as semi-arid in the De Martonne classification. The Urmia station is located at 45.06°N and 37.66°E at an altitude of 1328 m (Salahi et al., 2017). Furthermore, the city of Kerman is located in southeastern Iran, and the climate of this region is classified as dry in the De Martonne classification. The Kerman station is located at 56.96°N and 30.26°E at an altitude of 1754 m (Mazidi et al., 2021).

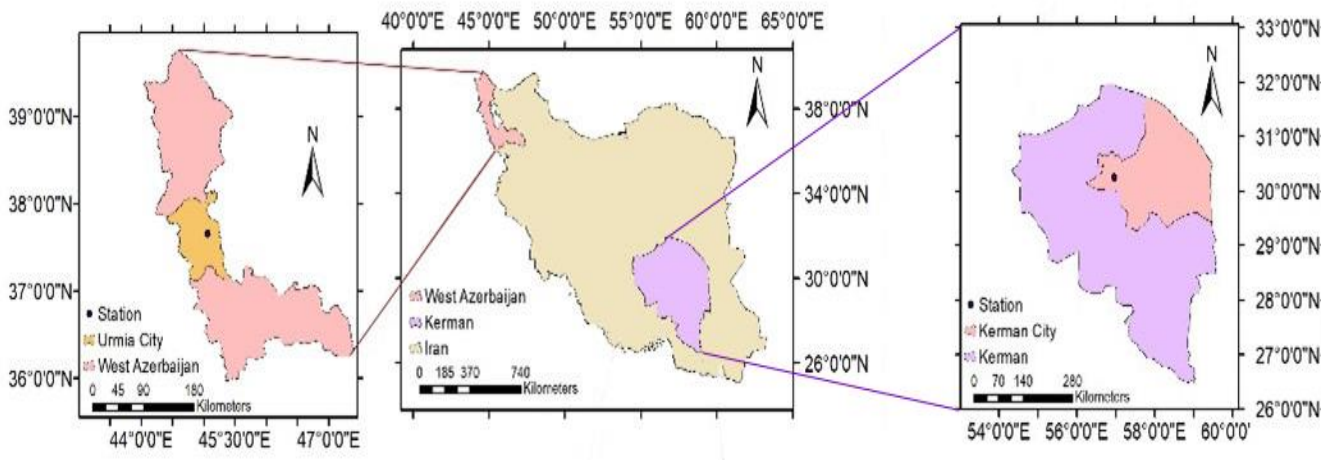


**Fig. 1** Location of the studied stations

### 2.2 The FAO Penman-Monteith equation

In this research, the standard FAO Penman-Monteith method for calculating the reference crop evapotranspiration is considered as the baseline method (Equation 1). The FAO Penman-Monteith equation, Eq. 1, (Allen et al., 1998), which combines radiometric and aerodynamic variables, has been recommended by the Food and Agriculture Organization of the United Nations (FAO) for evaluating $ET_0$ in different climates around the world (Fan et al., 2016).

$$ET_0 = \frac{0.408\,\Delta(R_n - G) + \gamma \frac{900}{T_{min}+273} U_2 (e_s - e_a)}{\Delta + \gamma(1 + 0.34U_2)} \quad (1)$$

In Eq. 1, $ET_0$ is the reference crop evapotranspiration (mm/d), $\Delta$ is the slope of the saturation vapor pressure curve (kPa/°C), $R_n$ is the net solar radiation (MJ/m$^2$.d$^1$), G is the soil heat flux density (MJ/m$^2$.d), $\gamma$ is the psychometric constant (kPa/°C), $T_{min}$ is the mean air temperature at a 2 m height (C$^{-1}$), $U_2$ is the mean daily wind speed at a 2 m height (m/s), $e_s$ is the saturation vapor pressure (kPa), and $e_a$ is the actual vapor pressure (kPa).

### 2.3 Interpolation Functions

In this study, four interpolation functions were used: Spline, Cubic Spline, Bezier, and Composite Bezier. Spline is a special type of piecewise polynomial. If the polynomials are of degree three, the function in question is called a cubic spline, in which the first derivative is continuous but the second derivative is not. In the Bezier function, unlike the common interpolation methods where the curves pass through the given data points, the curves do not pass through the points and the points are used only to control the shape of the curve (Baydas and Karakas, 2019). The composite Bezier curve in geometric modeling is a spline made up of Bezier curves.

### 2.4 Multilayer perceptron networks

A multilayer perceptron (MLP) neural network typically consists of multiple layers and neurons. The first and lowest layer is the input layer where external information is received. The last or highest layer is the output layer where the problem is solved. The input and output layers are separated by one or more intermediate layers called the hidden or middle layer. The neurons in adjacent layers are typically fully connected by non-cyclic arcs from the lower layer to the upper layer (Taud and Mas, 2018). In the current study, two hidden layers and 200 training cycles were used.

### 2.5 Stochastic Gradient Descent

Stochastic Gradient Descent (SGD) is an algorithm that uses gradient descent to minimize the objective function and create a regression model. The algorithm starts with a random selection of a starting point from the training data, and then iteratively adjusts the model to find the point of minimum cost. SGD repeatedly updates the model variables using gradient information on a small random batch of samples, which reduces the computational cost and makes it suitable for solving large-scale problems. This method has become an algorithm for training many machine learning models due to its low computational overhead and easy implementation (Lin and Rosasco, 2017). Regularization is used to prevent overfitting, and a base value is added to the cost function until an optimal result is obtained. The algorithm selects a cluster and calculates the gradient of that cluster (Bottou, 2010). In this study, the implemented model has three hidden layers, each with 50 neurons.

### 2.6 Remote sensing variables

Four remote sensing variables including nighttime land surface temperature (LST-N), daytime land surface temperature (LST-D), leaf area index (LAI) and normalized difference vegetation index (NDVI) were extracted from MODIS sensor images using the Google Earth Engine. In the MODIS sensor, more complete information was available for the stations of Kerman and Urmia compared to other sensors. Given that satellite data are available on a multi-day basis, these data need to be interpolated to obtain daily data. Since significant research has not been done on the downscaling or temporal interpolation of satellite data, this study compared four interpolation functions. For the interpolation of multi-day data and their conversion to daily data in this study, four interpolation functions including spline, cubic spline, Bezier and composite Bezier were used. The execution scenarios for the two methods of MLP and the combination of multilayer perceptron and stochastic gradient descent (MLP-SGD) at the Urmia and Kerman stations using four interpolation methods are presented in Table 1. The MLP-SG model scenarios are exactly similar to the scenarios in Table 1. The modeling was performed in three categories including the combined use of temperature and vegetation variables, the use of temperature variables, and the use of vegetation variables, using the data from four interpolation methods. Table 1 shows the input combination for the MLP and MLP-SGD model scenarios. Also, in the implementation of the models in this study, 70% of the data was used for training and the remaining 30% for model testing. The overall trend of the implementation of this study is shown in Fig. 2.

**Table 1** Composition of the studied model inputs

| No. | Scenario | LST-N | LST-D | LAI | NDVI |
|---|---|---|---|---|---|
| 1 | S-MLP-1 | * | * | * | * |
| 2 | S-MLP-2 | * | * | | |
| 3 | S-MLP-3 | | | * | * |
| 4 | CS-MLP-1 | * | * | * | * |
| 5 | CS-MLP-2 | * | * | | |
| 6 | CS-MLP-3 | | | * | * |
| 7 | B-MLP-1 | * | * | * | * |
| 8 | B-MLP-2 | * | * | | |
| 9 | B-MLP-3 | | | * | * |
| 10 | CB-MLP-1 | * | * | * | * |
| 11 | CB-MLP-2 | * | * | | |
| 12 | CB-MLP-3 | | | * | * |

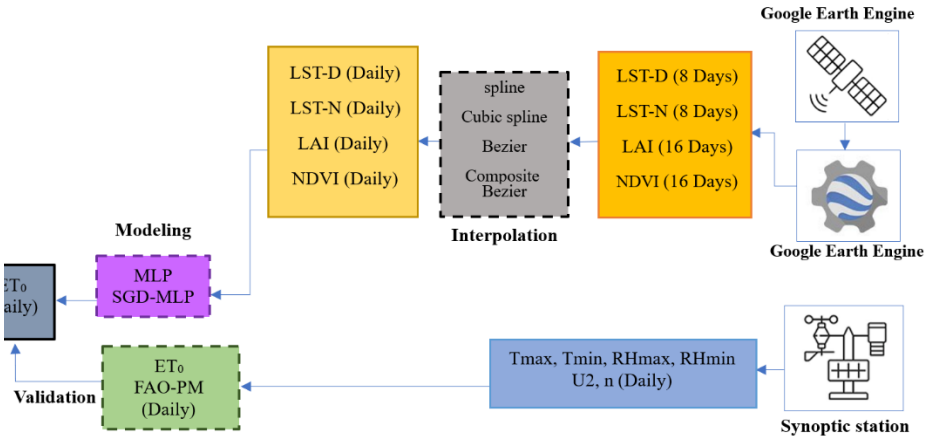


**Fig. 2** The general process of research implementation

### 2.7 Performance functions

$ET_0$ values resulting from four interpolation methods and different scenarios were evaluated using error variables. The error values of the types of models were examined using the statistical variables mean bias error (MBE), root mean squared error (RMSE), coefficient of determination ($R^2$), mean absolute percentage error (MAPE), Nash-Sutcliffe coefficient (NS) and Willmott's index of agreement (WI), using equations (2) to (7). In all equations, x represents the observed values, i.e. $ET_0$ from the FAO-56 equation, and y represents the calculated $ET_0$ values from the models.

$$MBE=\frac{1}{n}\sum_{i=1}^{n}(y_i-x_i)^2 \quad (2)$$

$$RMSE=\sqrt{\frac{1}{n}\sum_{i=1}^{n}(y_i-x_i)^2} \quad (3)$$

$$R^2=1-\frac{\sum(y_i-x_i)^2}{\sum(x_i-\bar{x}_i)^2} \qquad 0<R^2\leq 1.00 \quad (4)$$

$$MAPE=\frac{1}{n}\sum_{i=1}^{n}\left|\frac{x_i-y_i}{x_i}\right|*100 \qquad 10\%<MAPE\leq 50\% \quad (5)$$

$$NS=1-\left[\frac{\sum_i^n(y_i-x_i)^2}{\sum_i^n(x_i-\bar{x}_i)^2}\right] \qquad 0.4<NS\leq 1.00 \quad (6)$$

$$WI=1-\left[\frac{\sum_i^n(y_i-x_i)^2}{\sum_i^n(|y_i-\bar{x}_i|+|x_i-\bar{x}_i|)^2}\right] \qquad 0.30<WI\leq 1.00 \quad (7)$$

### 3.1 Modeling results at the Urmia station

According to $ET_0$ modeling using remote sensing variables, for determining the base values, meteorological parameters was obtained from two stations of Urmia and Kerman, and $ET_0$ was calculated using the FAO56-PM method. Four parameters derived from the MODIS sensor including LST-D, LST-N, NDVI, and LAI were interpolated using four spline, cubic spline, Bezier, and composite Bezier functions and converted to daily data. Daily remote sensing data were used as input to the MLP and SGD-MLP models in 12 scenarios. The scenarios are divided into three categories: 1. a combination of land surface temperature and vegetation indices, 2. based on day and night land surface temperature, and 3. based on vegetation indices.

**Table 2** Statistical results of MLP model in Urmia

| Urmia Models | $R^2$ | RMSE (mm/day) | NS | WI | MAPE | (mm/day) MBE |
|---|---|---|---|---|---|---|
| S-MLP-1 | 0.903 | 0.797 | 0.885 | 0.969 | 20.784 | -0.296 |
| S-MLP-2 | 0.901 | 0.785 | 0.889 | 0.967 | 32.674 | 0.161 |
| S-MLP-3 | 0.615 | 1.549 | 0.566 | 0.851 | 67.575 | 0.501 |
| CS-MLP-1 | 0.903 | 0.796 | 0.885 | 0.969 | 20.789 | -0.296 |
| CS-MLP-2 | 0.901 | 0.784 | 0.889 | 0.968 | 32.68 | 0.163 |
| CS-MLP-3 | 0.616 | 1.535 | 0.574 | 0.854 | 65.847 | 0.472 |
| B-MLP-1 | 0.755 | 1.174 | 0.751 | 0.922 | 42.775 | 0.09 |
| B-MLP-2 | 0.753 | 1.187 | 0.746 | 0.918 | 44.887 | 0.134 |
| B-MLP-3 | 0.233 | 2.105 | 0.2 | 0.594 | 106.737 | 0.425 |
| CB-MLP-1 | 0.869 | 0.896 | 0.855 | 0.96 | 24.682 | -0.277 |
| CB-MLP-2 | 0.869 | 0.897 | 0.855 | 0.957 | 37.801 | 0.232 |
| CB-MLP-3 | 0.830 | 0.977 | 0.828 | 0.949 | 36.063 | -0.043 |

The statistical results of the models implemented in this study at the test stage are presented. According to Table 2 at the Urmia station and the MLP model, the highest coefficient of determination is 0.903 in the S-MLP-1 and CS-MLP-1 scenarios, which is the result of using all four parameters LST-D, LST-N, NDVI, and LAI with spline and cubic spline

interpolation. However, the lowest RMSE error of 0.784 mm/day occurred in the CS-MLP-2 model, which has two inputs of daytime and nighttime LST. In the Urmia station and the SGD-MLP model, the highest coefficient of determination in the CS-SGD-MLP-2 scenario is 0.899, which is the result of using two inputs of day and night LST with cubic spline interpolation (Table 3). Meanwhile, the lowest RMSE error in the GD-MLP-S-2 model is 0.901 mm/day, which is the result of using two inputs of day and night LST with spline interpolation.

**Table 3** Statistical results of SGD-MLP model in Urmia

| Urmia Models | $R^2$ | RMSE (mm/day) | NS | WI | MAPE | MBE (mm/day) |
|---|---|---|---|---|---|---|
| S-SGD-MLP-1 | 0.889 | 1.343 | 0.674 | 0.89 | 30.869 | -0.911 |
| S-SGD-MLP-2 | 0.897 | 0.901 | 0.853 | 0.952 | 30.197 | -0.248 |
| S-SGD-MLP-3 | 0.031 | 2.318 | 0.029 | 0.246 | 127.021 | 0.096 |
| CS-SGD-MLP-1 | 0.872 | 1.112 | 0.777 | 0.913 | 57.393 | 0.078 |
| CS-SGD-MLP-2 | 0.899 | 1.256 | 0.715 | 0.881 | 46.512 | -0.398 |
| CS-SGD-MLP-3 | 0.605 | 1.721 | 0.465 | 0.741 | 56.837 | -0.493 |
| B-SGD-MLP-1 | 0.594 | 1.953 | 0.311 | 0.543 | 86.905 | -0.339 |
| B-SGD-MLP-2 | 0.503 | 2.152 | 0.164 | 0.502 | 81.23 | -0.702 |
| B-SGD-MLP-3 | 0.298 | 2.172 | 0.148 | 0.432 | 92.981 | -0.435 |
| CB-SGD-MLP-1 | 0.850 | 1.101 | 0.781 | 0.918 | 51.816 | -0.030 |
| CB-SGD-MLP-2 | 0.859 | 1.245 | 0.720 | 0.883 | 49.243 | -0.211 |
| CB-SGD-MLP-3 | 0.789 | 1.757 | 0.442 | 0.664 | 88.989 | -0.142 |

### 3.2 Modeling results at the Kerman station

The statistical results of the Kerman station are presented in the following. In Table 4, the MLP model has the highest simultaneous coefficient of determination in the two scenarios of S-MLP-1 and CS-MLP-1, amounting to 0.835, which is the result of using all four variables with spline interpolation and cubic spline. Meanwhile, the lowest RMSE error in the CS-MLP-1 model occurred at 1.098 mm/day, with four input variables and cubic spline interpolation.

Table 4 Statistical results of MLP model in Kerman

| Kerman Models | $R^2$ | RMSE (mm/day) | NS | WI | MAPE | MBE (mm/day) |
|---|---|---|---|---|---|---|
| S-MLP-1 | 0.832 | 1.099 | 0.816 | 0.949 | 18.214 | -0.329 |
| S-MLP-2 | 0.835 | 1.107 | 0.813 | 0.95 | 18.155 | -0.363 |
| S-MLP-3 | 0.294 | 2.262 | 0.22 | 0.731 | 40.525 | -0.33 |
| CS-MLP-1 | 0.832 | 1.098 | 0.816 | 0.949 | 18.233 | -0.324 |
| CS-MLP-2 | 0.835 | 1.107 | 0.813 | 0.95 | 18.158 | -0.363 |
| CS-MLP-3 | 0.295 | 2.259 | 0.222 | 0.732 | 40.434 | -0.326 |
| B-MLP-1 | 0.741 | 1.307 | 0.739 | 0.917 | 25.118 | -0.094 |
| B-MLP-2 | 0.728 | 1.343 | 0.725 | 0.917 | 25.054 | -0.094 |
| B-MLP-3 | 0.274 | 2.38 | 0.136 | 0.693 | 40.806 | -0.776 |
| CB-MLP-1 | 0.814 | 1.135 | 0.803 | 0.944 | 19.973 | -0.254 |
| CB-MLP-2 | 0.814 | 1.172 | 0.791 | 0.942 | 19.724 | -0.375 |
| CB-MLP-3 | 0.296 | 2.297 | 0.195 | 0.732 | 39.434 | -0.455 |

In the continuation of the Kerman station and in the study of the SGD-MLP model, in Table 5 the highest coefficient of determination in the S-SGD-MLP-2 scenario is 0.832, which is the result of using two inputs of day and night LST with spline interpolation. Meanwhile, the lowest RMSE error in the S-GD-MLP-2 model is 1.143 mm/day, which is the result of using two inputs of day and night LST with spline interpolation.

### 3.3 Comparison of scenario performance

Given that a single statistical indicator cannot be used to identify the best model, the Taylor diagram is a method based on three statistical parameters that allow for their simultaneous comparison. This diagram can provide a summary of the patterns' conformity with each other in terms of correlation, root mean square error, and variance ratio, which was developed by Taylor (2001). Considering the Taylor diagrams in Fig. 3, in the Urmia station (Fig. 3b), the best models are the fourth scenario modeling with MLP using all four parameters and cubic spline interpolation, and the second scenario,

modeling with SGD-MLP using day and night LST and spline interpolation. In the Kerman station (Fig. 3a), the best models are the fifth scenario modeling with MLP using day and night LST and cubic spline interpolation, and the second scenario modeling with SGD-MLP using day and night LST and spline interpolation.

**Table 5** Statistical results of SGD-MLP model in Kerman

| Kerman Models | $R^2$ | RMSE (mm/day) | NS | WI | MAPE | (mm/day) MBE |
|---|---|---|---|---|---|---|
| S-SGD-MLP-1 | 0.826 | 1.482 | 0.665 | 0.884 | 21.882 | -0.856 |
| S-SGD-MLP-2 | 0.832 | 1.143 | 0.801 | 0.946 | 19.232 | -0.431 |
| S-SGD-MLP-3 | 0.276 | 2.19 | 0.269 | 0.663 | 44.639 | -0.199 |
| CS-SGD-MLP-1 | 0.830 | 1.294 | 0.745 | 0.899 | 28.521 | -0.072 |
| CS-SGD-MLP-2 | 0.806 | 1.671 | 0.574 | 0.783 | 36.46 | -0.219 |
| CS-SGD-MLP-3 | 0.206 | 2.894 | -0.277 | 0.618 | 44.071 | -1.613 |
| B-SGD-MLP-1 | 0.513 | 1.995 | 0.393 | 0.708 | 50.898 | 0.617 |
| B-SGD-MLP-2 | 0.697 | 1.791 | 0.511 | 0.77 | 46.896 | 0.598 |
| B-SGD-MLP-3 | 0.120 | 2.484 | 0.059 | 0.56 | 54.761 | -0.026 |
| CB-SGD-MLP-1 | 0.797 | 1.584 | 0.618 | 0.821 | 34.205 | -0.257 |
| CB-SGD-MLP-2 | 0.810 | 1.368 | 0.715 | 0.886 | 28.181 | -0.246 |
| CB-SGD-MLP-3 | 0.268 | 2.325 | 0.176 | 0.671 | 41.213 | -0.708 |

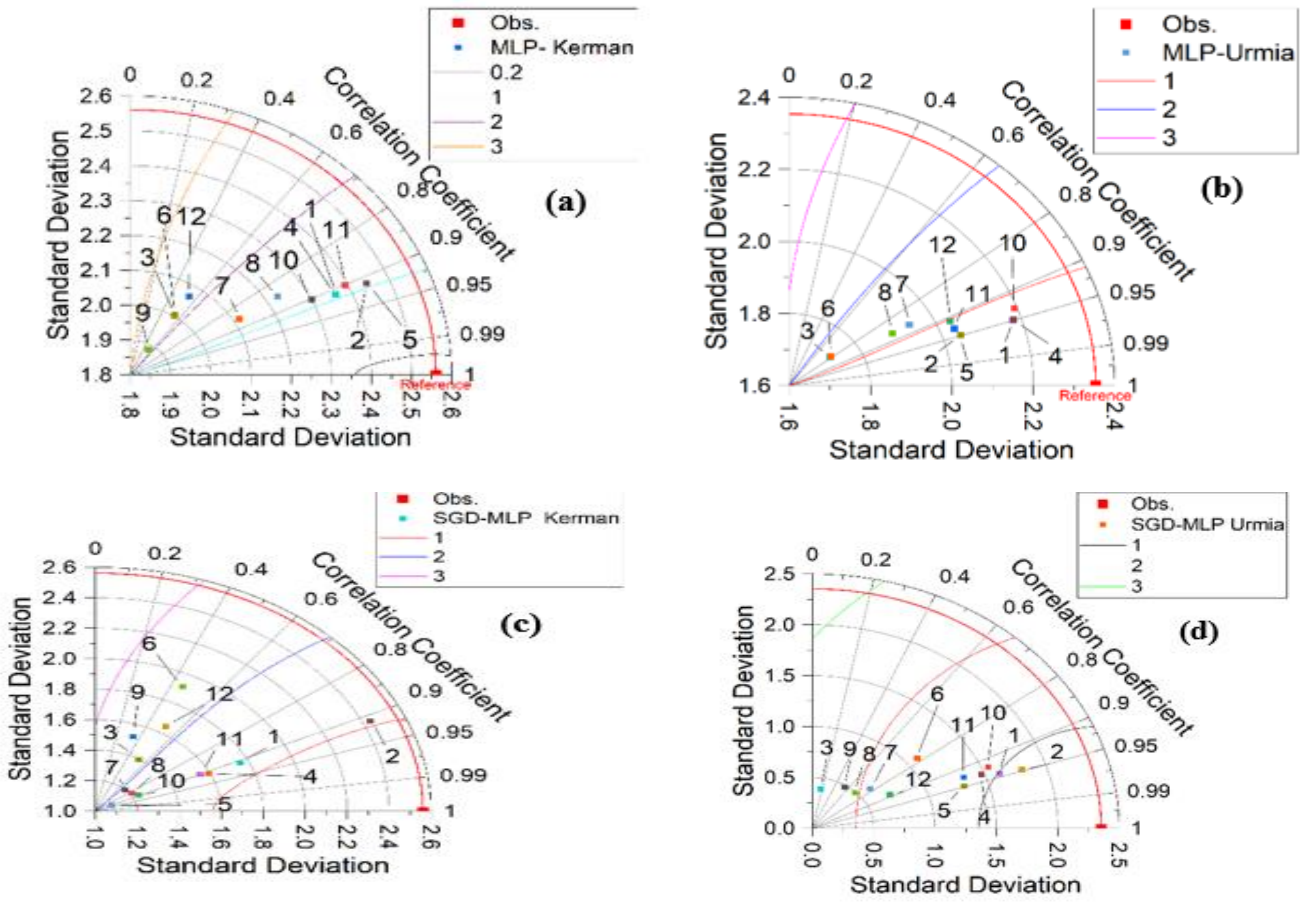


**Fig. 3** Taylor diagram of models: a) MLP in Kerman, b) MLP in Urmia, c) SGD-MLP in Kerman, and d) SGD-MLP in Urmia

In addition, in Fig. 4, the comparison of the best models for each station is shown in a scatter plot to examine the data dispersion. In the Urmia station, the difference between the best MLP and SGD-MLP models is evident. The scatter plot of the blue points, which are related to the CS-MLP-1 model with a coefficient of determination of 0.614 and the S-SGD-MLP-2 model with a coefficient of determination of 0.898, shows that the spline interpolation in the Urmia station has

performed better, and the fitting line of this model is closer to the first quadrant bisector. In the Kerman station, the best models are very close to each other. The linear regression of the S-SGD-MLP-2 model with a coefficient of determination of 0.831 and the CS-MLP-2 model with a coefficient of determination of 0.835, shows that the cubic spline interpolation in the Kerman station has performed better. It seems that the performance of the interpolation functions varies in each climate.

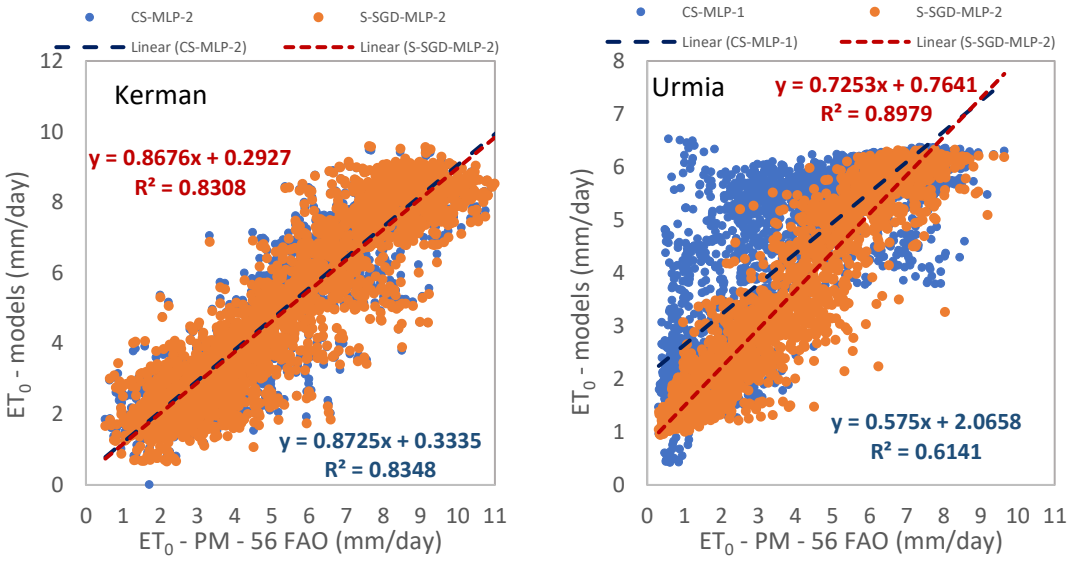


**Fig. 4** Comparison of daily reference evapotranspiration with top models

Talebi et al. (2024) used land surface temperature (LST) data during the day and night, as well as average land surface temperature during the day and night, to estimate $ET_0$. They implemented two random forest (RF) and genetic algorithm-improved random forest (GA-RF) models at the Tabriz and Rasht stations. Their results showed that the GA-RF model performed better at both the Tabriz and Rasht stations, with RMSE values of 0.516 and 0.868 mm/day, respectively. The lowest RMSE values in the present study were 0.78 in Urmia and 1.1 mm/day in Kerman. The difference is due to the use of vegetation variables with lower correlation with evapotranspiration. Additionally, Granata et al. (2024) used innovative algorithms to predict $ET_0$ in the central Agropontinese region of Italy and found that the multilayer perceptron-random forest (MLP-RF) model, with only mean temperature, maximum relative humidity, and shortwave solar radiation as inputs, produced good results for a 60-day forecast, with a mean absolute percentage error (MAPE) of 8.356%. In the present study, without using meteorological data and using only remote sensing data with a lower correlation with evapotranspiration, the MAPE was around 18.1 in Kerman and 30.1 in Urmia.

Zhang et al. (2018) estimated reference evapotranspiration based on remote sensing data in northwestern China. The results showed that LST can be used for accurate estimation of $ET_0$ with high coefficients of determination ($R^2$ from 0.897 to 0.915). Rangaswamy and Kumar (2018) used LST data to estimate temperature in evapotranspiration estimation equations and found that $LST_{day}$ and $LST_{night}$ correspond 82% and 84% with $T_{max}$ and $T_{min}$, respectively, and the use of these satellite variables in evapotranspiration estimation was successful. Talebi et al. (2023) implemented stochastic gradient descent (SGD) to optimize multilayer perceptron (MLP) and develop SGD-MLP for daily $ET_0$ estimation at Tabriz (semi-arid climate) and Babolsar (humid climate) stations in Iran. Satellite imagery data from 2003 to 2021, including day and night land surface temperature (LST), normalized difference vegetation index (NDVI), leaf area index (LAI), and fraction of absorbed photosynthetically active radiation (FPAR) from MODIS sensor, were used. They performed modeling in three categories, based on LST, vegetation indices, and a combination of LST and vegetation indices. According to the results, SGD-MLP-3 with input variables of day and night LST, mean LST, LAI, NDVI, and FPAR obtained the most accurate results with RMSE = 0.417 mm/day, WI = 0.973 for Tabriz and 0.754 mm/day, 0.922 for Babolsar station. Finally, day, night, and mean LST were suggested as the most influential parameters for $ET_0$ estimation. The difference in the results of this study compared to the present study may be due to the greater number of input variables, which resulted in lower error in the current study.

## 4. Conclusion

To solve the issue of daily lack of remote sensing data, four interpolation functions were used in this study to convert 8-day land surface temperature (LST-D/N) and 16-day vegetation indices (NDVI and LAI) data to daily data for daily $ET_0$ estimation. The calculated $ET_0$ values with the FAO-56 PM equation were considered as the reference. Then, using two models of MLP and SGD-MLP, the reference evapotranspiration was modeled in three categories: a combination of surface temperature, a combination of LAI and NDVI variables, and a combination of all four parameters. The results of this study showed:

1. In the Urmia station and the MLP method, the MLP-4 scenario, i.e., the use of all four parameters and with cubic spline interpolation, and in the SGD-MLP method, the SGD-MLP-2 scenario, i.e., the model using day and night LST and with spline interpolation, were the best models.

2. In the Kerman station, with the MLP-5 scenario, i.e., the use of day and night LST and with cubic spline interpolation, and in the SGD-MLP modeling, the SGD-MLP-2 scenario, i.e., with the use of day and night LST and with spline interpolation, were the best models.

3. In general, the MLP model with spline-interpolated data and the SGD-MLP model with cubic-spline-interpolated data performed better. Finally, the best model at the Urmia station was the S-SGD-MLP-2 scenario, and at the Kerman station was the CS-MLP-2. Also, the statistical results showed that the MLP model had fewer errors compared with the SGD-MLP model in similar scenarios.

**Statements and Declarations**

**Data availability**

The data can be sent by email from the Corresponding author upon request.

**Conflicts of interest**

The author of this paper declared no conflict of interest regarding the authorship or publication of this paper.

**Author contribution**

P. Amirzehni: Data collection, data visualization, data analysis, and interpretation; S. Samadianfard: Research design, interpretation of results; A. Nazmi: Structural and content editing; A. A. Sadraddini: Drafting and revision.

**AI Use Disclosure**

During the preparation of this manuscript, the authors used ChatGPT for language translation. All content has been carefully reviewed and revised by the authors, who take full responsibility for the final version of the manuscript.

**References**


Allen, R., Pereira, L., Raes, D., & Smith, M. (1998). Crop evapotranspiration-Guidelines for computing crop water requirements- FAO Irrigation and drainage paper 56, FAO, Rome, 300: D05109.

Aghelpour, P., Bahrami-Pichaghchi, H., & Karimpour, F. (2022a). Estimating daily rice crop evapotranspiration in limited climatic data and utilizing the soft computing algorithms MLP, RBF, GRNN, and GMDH. *Complex., 1–18*. DOI: 10.1155/2022/4534822

Aghelpour, P., Varshavian, V., Pour, M. K., & Hamedi, Z. (2022b). Comparing three types of data-driven models for monthly evapotranspiration prediction under heterogeneous climatic conditions. *Sci. Report., 12*(1). DOI: 10.1038/s41598-022-22272-3

Ahmadpari, H., Safavi Gerdini, M., & Ebrahimi, M. (2019). An appropriate method for estimating potential evapotranspiration in the absence of meteorological data (The case study of Khorrambid Township in Fars Province). *Land Manage. J.*, *7*(2), 223-230. DOI: 10.22092/lmj.2019.120559

Amirzehni, P., Samadianfard, S., Nazemi, A., & Sadraddini, A. (2023). Evaluating capabilities of the spline and cubic spline interpolation functions in reference evapotranspiration estimation implementing satellite image data. *Earth Sci. Inform.*, *16*(4), 3779-3795. DOI: 10.1007/s12145-023-01127-z

Baydas, S., & Karakas, B. (2019). Defining a curve as a Bezier curve. *J. Taibah Univ. Sci.*, *13*(1), 522-528. DOI: 10.1080/16583655.2019.1601913

Bellido-Jiménez, J. A., Estévez, J., & García-Marín, A. P. (2023). Reference evapotranspiration projections in Southern Spain (until 2100) using temperature-based machine learning models. *Comput. Electron. Agri., 214*, 108327. DOI: 10.1016/j.compag.2023.108327

Bottou, L. (2010). Large-scale machine learning with stochastic gradient descent. In: Lechevallier, Y., Saporta, G. (eds) Proceedings of COMPSTAT'2010. Physica-Verlag HD. DOI: 10.1007/978-3-7908-2604-3_16

Ebrahimipak, N., Tafteh, A., Egdarnejad, A., & Asadi Kapourchal, S. (2018). Determination of monthly evapotranspiration coefficients of winter wheat by different methods of estimating evapotranspiration and evaporation pan in Qazvin plain. *Irrig. Water Eng.*, *8*(4), 107-121. [In Persian]

Falamarzi, Y., Palizdan, N., Huang, Y. F., & Lee, T. S. (2014). Estimating evapotranspiration from temperature and wind speed data using artificial and wavelet neural networks (WNNs). *Agri. Water Manage., 140*, 26–36. DOI: 10.1016/j.agwat.2014.03.014

Fan, J., Wu, L., Zhang, F., Xiang, Y., & Zheng, J. (2016). Climate change effects on reference crop evapotranspiration across different climatic zones of China during 1956–2015. *J. Hydrol., 542*, 923-937. DOI: 10.1016/j.jhydrol.2016.09.060

Ferreira, L. B., Da Cunha, F. F., De Oliveira, R. A., & Filho, E. I. F. (2019). Estimation of reference evapotranspiration in Brazil with limited meteorological data using ANN and SVM – A new approach. *J. Hydrol., 572*, 556–570. DOI: 10.1016/j.jhydrol.2019.03.028

Granata, F., Di Nunno, F., & De Marinis, G. (2024). Advanced evapotranspiration forecasting in Central Italy: Stacked MLP-RF algorithm and correlated Nystrom views with feature selection strategies. *Comput. Electron. Agri., 220*, 108887. DOI: 10.1016/j.compag.2024.108887

Hashemi, M., & Sepaskhah, A. R. (2019). Evaluation of artificial neural network and Penman-Monteith equation for the prediction of barley standard evapotranspiration in a semi-arid region. *Theor. Appl. Climatol., 139(1–2)*, 275–285. DOI: 10.1007 / s00704-019-02966-x

Keshtegar, B., Abdullah, S. S., Huang, Y. F., Saggi, M. K., Khedher, K. M., & Yaseen, Z. M. (2022). Reference evapotranspiration prediction using high-order response surface method. *Theor. Appl. Climatol., 148(1–2)*, 849–867. DOI: 10.1007 /s00704-022-03954-4

Lin, J., & Rosasco, L. (2017). Optimal rates for multi-pass stochastic gradient methods. *J. Machine Learn. Res., 18*, 1–47. DOI: 10.48550/arXiv.1605.08882

Mazidi, A., Enayatpour, M, & Hosseini, S. S. (2021). A GIS-based agroecological model for sustainable agricultural production in arid and semi-arid areas: The case of Kerman Province. *Geogra. Human Relat.*, *4*(14). DOI: 10.22034/gahr.2021.287987.1565 [In Persian].

Pereira, L. S., Allen, R. G., Smith, M., & Raes, D. (2015). Crop evapotranspiration estimation with FAO56: Past and future. *Agri. Water Manage.*, *147*, 4-20. DOI: 10.1016/j.agwat.2014.07.031

Popovic, P. L., Gocić, M., Petković, K., & Trajković, S. (2023). Neural network based system in evapotranspiration time series prediction. *Earth Sci. Inform.*, *16*(1), 919–928. DOI: 10.1007/s12145-023-00935-7

Rangaswamy, S., & Kumar, D. N. (2018). Performance evaluation of satellite-based approaches for the estimation of daily air temperature and reference evapotranspiration. *Hydrol. Sci. J.*, *63*(9), 1347–1367. DOI: 10.1080/02626667.2018.1505046

Salahi, B., Goudarzi, M., & Hosseini, S. A. (2017). Prediction of climate parameter changes in the Urmia Lake watershed during the period 2030-2011. *Jo. Watershed Manage. Sci. Eng.*, *11*(37), 47-56. DOI: 20.1001.1.20089554.1396.11.37.3.7 [In Persian].

Talebi, H., Samadian Fard, S., & Valizadeh Kamran, K. (2024). The impact of land surface temperature from MODIS sensor on daily reference evapotranspiration estimation in two different climates. *Environ. Water Eng.*, *9*(3), 367-383. DOI: 10.22034/ewe.2022.366189.1815. 2 [In Persian].

Talebi, H., Samadianfard, S., & Kamran, K. V. (2023). Investigating the roles of different extracted parameters from satellite images in improving the accuracy of daily reference evapotranspiration estimation. *Appl. Water Sci.*, *13*(2). DOI: 10.1007/s13201-022-01862-6

Taud, H., & Mas, J. F. (2018). Multilayer perceptron (MLP). *Geomatic approaches for modeling land change scenarios*, 451-455. DOI: 10.1007/978-3-319-60801-3

Taylor, K. E. (2001). Summarizing multiple aspects of model performance in a single diagram. *J. Geophys. Res.*, *106*(7), 7183–7192. DOI: 10.1029/2000jd900719

Walls, S., Binns, A., Levison, J., & MacRitchie, S. (2020). Prediction of actual evapotranspiration by artificial neural network models using data from a Bowen ratio energy balance station. *Neur. Comput. Appl.*, *32*(17), 14001–14018. DOI: 10.1007 / s00521-020-04800-2

Zhang, Z., Gong, Y., & Wang, Z. (2018). Accessible remote sensing data based reference evapotranspiration estimation modelling. *Agri. Water Manage.*, *210*, 59–69. DOI: 10.1016/j.agwat.2018.07.039